![CAMBRIDGE UNIVERSITY PRESS]

Adaptive triple-fed antenna and thinned RF-chip integration into ultra thin flexible polymer foil

Serafin B. Fischer-Kennedy[1] (iD), Sefa Özbek[2], Shuo Wang[3], Markus Grözing[2], Jan Hesselbarth[1], Manfred Berroth[2] and Joachim N. Burghartz[3]

[1]Institute of Radio Frequency Technology, University of Stuttgart, Stuttgart, Germany; [2]Institute of Electrical and Optical Communications Engineering, University of Stuttgart, Stuttgart, Germany and [3]Institute for Nano and Microelectronic Systems, University of Stuttgart, Stuttgart, Germany

Abstract

Attaching a wireless transmission system comprising a radio frequency (RF)-chip and a dipole antenna to dielectric material of largely different permittivity leads to strong variation of the antenna feed impedance. Due to the severe impedance mismatch between the RF-chip and the antenna, the performance of the system may deteriorate drastically. The proposed antenna provides three feed points, which show respective feed-point match to 100 Ohm balanced feeds for three different dielectric environments (free-space and half-spaces of permittivity 4 and 42, respectively). Thereby, the RF-chip incorporates three 100 Ohm balanced output ports that are connected to the antenna from whom only one can be selected to provide the output signal. The respective other two output ports are shorted by an internal switching circuit that is controlled by external DC voltages. The measurement of the reflection coefficient of the stand-alone antenna and the chip agree well with the simulations, allowing to interconnect these two components. Further, the radiation pattern of the whole system is measured for two different scenarios showing good functionalities.

Introduction

This paper is a significantly extended version of [1] presented at the 16th European Conference on Antennas and Propagation and was published in its Proceedings. In [1], the concept and design of the antenna as well as stand-alone measurement results are presented. This paper, however, presents a flexible and adaptive wireless transmitter system that includes radiation pattern measurement for different electromagnetic (EM) environments. To the best of the authors' knowledge, such a system has not been reported previously.

Adaptive communication systems are essential for many Internet of Things and Radio Frequency Identification applications. The adaptivity relates to the EM environment in which the system operates, such as free-space, being attached to a parcel or package, or on the human body. Another aspect that contributes to adaptivity is mechanical flexibility, such as the ability to bend. The antenna's characteristics, including its feed impedance, can be significantly affected by these factors, which can lead to a drastic deterioration of system performance.

The impact of bending on a wearable patch antenna is studied in [2], while [3] examines a stretchable and flexible antenna able to be attached on human skin. Changes in antenna performance caused by variations in the dielectric surrounding the antenna can be even more significant than bending. These changes affect both the input impedance and the radiation characteristics of the antenna. Variations in the radiation pattern, such as changes in gain, can negatively impact the wireless link, while changes in input impedance can have a detrimental impact on overall system performance. This problem is discussed in [4], where a microstrip dipole is covered with dielectrics of different values of permittivity. Various approaches have been proposed to address this problem, such as using a dielectric load as an insulator to maintain matching, as outlined in [5] and [6]. This technique increases the form factor (thickness) of the antenna, which may be undesirable. Another approach is using a tuneable matching network, as in [7], but this increases technological complexity (MEMS in [7]), cost, and mechanical thickness. In [8], switching the feed position along the dipole radiator is used to provide impedance matching. Some alternative scenarios may include a metal surface in close proximity of the antenna. The antenna proposed in [9] uses two different resonant modes, one when operating in free-space and one for a nearby metal surface, to achieve impedance matching in both cases.

The system presented in this paper operates at around 5.5 GHz; it consists of a single chip, which has been thinned down to about 40 μm, and an antenna, all embedded into a thin foil
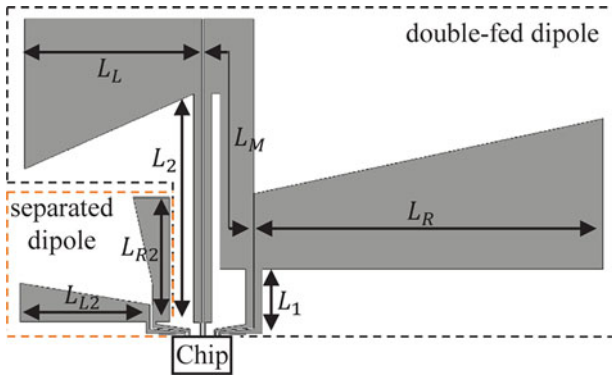
Figure 1. The layout of the complete dipole-based antenna structure [1].

Figure 2. Simplified schematic view of the power amplifier.

Figure 3. Momentum view of transformers, inductors, and interconnections.

(thickness 50 μm). It is worth to note that the thinned chips are mechanically flexible and can be embedded into the foil using advanced technology [10–12]. The integration of RF amplifier and antenna within the foil has been demonstrated in [13]. The system remains functional when the flexible foil is directly attached to different dielectric bodies. To keep the chip complexity low, the antenna is designed to have three feeds, one of which always provides a good match to a 100 Ohm balanced feed-port, regardless of the dielectric environment. Since the antenna structure is physically much larger than the chip, the three antenna feed-ports shall be co-located within a 1.4 mm distance, to be connected easily to the chip (the chip contains the one-to-three switch). This requirement imposes consideration of the feedlines and their impact on the antenna's characteristics.

The second and third sections show the concept of the proposed antenna and the RF-chip, respectively. The used flexible foil technology is given in the fourth section. Then, the stand-alone prototypes of the antenna and the RF-chip with their measurements are presented in the fifth and sixth section. In the seventh section, the prototype and the measurement of the whole system is introduced. Finally, the last section concludes the whole work.

The simulations of the antenna were performed using CST Microwave Studio software.

Concept of the antenna

The antenna is designed to be thin and mechanically flexible, and it is implemented in a foil. A single-layer metal dipole-like structure is chosen for a decent bandwidth. The antenna is intended to provide 100 ohm balanced feeds to the chip. Largely different environments (air, half-space of permittivity 4 and 42, respectively) would lead to largely different dipole sizes when considering three center-fed dipoles. To achieve a compact antenna design, a double-fed dipole with an enclosed second dipole is chosen. Figure 1 depicts the layout of the antenna connected to the RF-chip.

Double-fed dipole

A double-fed dipole antenna (see multiple-fed dipoles in [8, 14]) is considered (within the black dashed border in Fig. 1) for the two scenarios with the lowest permittivity, air and butter. This combines the two physically larger dipoles into a single structure, resulting in a compact device. Switches (within the RF-chip) are located at the respective ends of the feedlines 1 and 2, which optionally open-circuit the amplifier output and short-circuit the line (see Fig. 2).
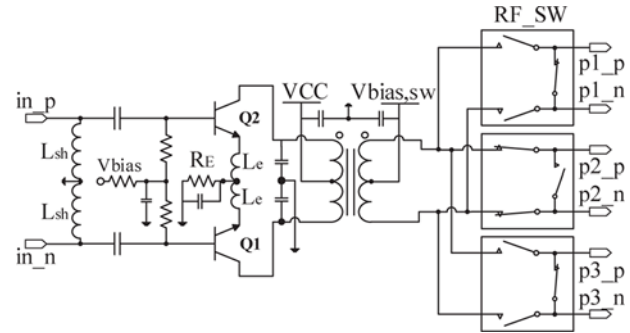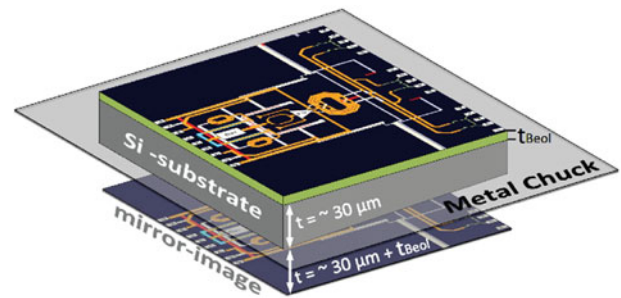
If one line (e.g., 2 with length L_2) is short-circuited, (scenario 1) the other one (line 1 with length L_1) serves as the feedline. If this feedline does not belong to the radiating structure, the resonant frequency is determined by lengths L_L, L_M, L_R, and L_2. If the other line (line 1) is short-circuited and line 2 serves as feedline, the resonant frequency is determined by L_L, L_M, L_R, and L_1. If $L_1 \neq L_2$, then different resonant lengths are possible. Or in this case, if the wavelength changes (by changing the material in the environment) from scenario 1 to 2, the resonant frequency remains the same by choosing the appropriate lengths of L_1 and L_2. Unfortunately, because of the asymmetry, the lengths of the two arms will differ, causing the current distribution to be no longer symmetric with respect to the feed point. This means that the even part of the current distribution does not disappear at the feed point. As a result, the currents flowing through each of the conductors of the feedline will be different in magnitude, and their phase difference will not be 180 degrees. This leads to the electric and magnetic fields of the two-conductor feedline having significant non-transversal components. This in turn leads to the radiation of the feedline as pointed out in [15], disabling the aforementioned considerations. Thus, different resonant length can be obtained only if the even mode is suppressed. In [16], it is shown how the even mode on the feedline of an asymmetrical driven dipole can be suppressed using a in-series load impedance, placed somewhere along the dipole. If the double-fed dipole is viewed as an asymmetrically fed dipole, the load line is a reactive load. As a consequence, for certain lengths of L_1 and L_2, as well as a certain feed and load positions, an antenna design can be found that allows the double-fed antenna to be resonant for two different EM environments. To the best of the authors' knowledge, this approach is first mentioned in [1]. More details on the concept and how to find the respective lengths and feed positions are available in [1].
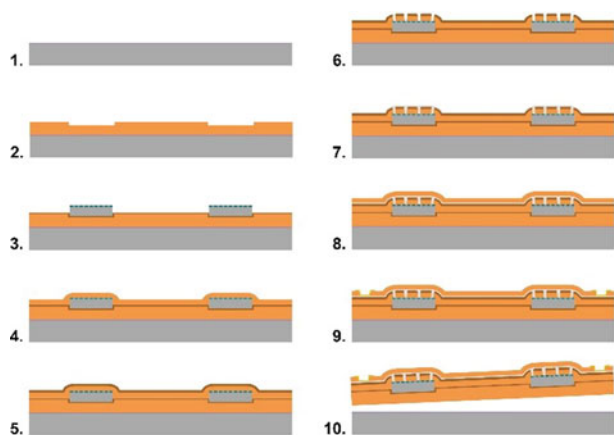
Figure 4. The process flow of the CFP technology [1]: (1) Surface preparation for temporary bonding; (2) spin coating with polyimide (PI2611), followed by production of cavities; (3) coating a thin BCB layer as glue and placing the chips using a fine placer; (4) embedding the chip with PI; (5) BCB coating as an adhesive layer for subsequent metal sputtering (6) opening the chip contact pads; (7) AlSiCu sputtering and structuring; (8) embedding the metal layer with PI; (9) opening the external contact pads or Antenna area if required by lithography and plasma etching; and (10) releasing hybrid CFP from the silicon carrier.

Separated dipole

Since designing a triple-fed dipole antenna using the same approach (as in the previous section) would be too involved, the third scenario is handled by a separate dipole (within the orange dashed border in Fig. 1). As this scenario belongs to the highest permittivity environment, this dipole is small. To keep the overall design compact, this dipole is placed very close to the double-fed dipole and therefore strongly field coupled. Thus, field simulations are used to optimize the shape of the separate dipole. Similar to the double-fed dipole, this dipole also features an on-chip switch, which short-circuits the feedline when not in use.

Concept of the RF-chip

In this study, a high-speed and cost-driven 95 GHz-fmax 250 nm SiGe BiCMOS HBT (IHP process SGB25V) technology is used for energy-efficient power amplifier (PA) operating at 5–6 GHz. The simplified schematic of the differential PA is illustrated in Fig. 2. A single-path PA is implemented instead of a three-path structure for low-area occupation as the system's topology is intended to use only one output port feeding. In contrast, the remaining differential output ports are shorted and isolated from the amplifier using the fully integrated isolated n-type metal-oxide semiconductor (NMOS) switches with the series/shunt configuration topology. The operating point of the PA has already been calculated in the previous study of three-path amplifier design [17]. Therefore, as part of this study, an output matching network is optimized for a single-path PA structure and evaluated, considering various substrate thicknesses and backside materials. The output matching is performed using an octagonal shape 2:2 transformer and shunt capacitors at the primary side of the transformer, while shunt inductors and series capacitors are used for the input matching. As illustrated in Fig. 3, all passive components in one view, including power lines, interconnects, inductors, and transformers, are extracted using the EM simulator tool of Advanced Design System (ADS) Momentum to improve the accuracy of the models. A perfect electric conductor and insulating material (FR4) are preferred

Table 1. Measured/extracted properties of the dielectric materials

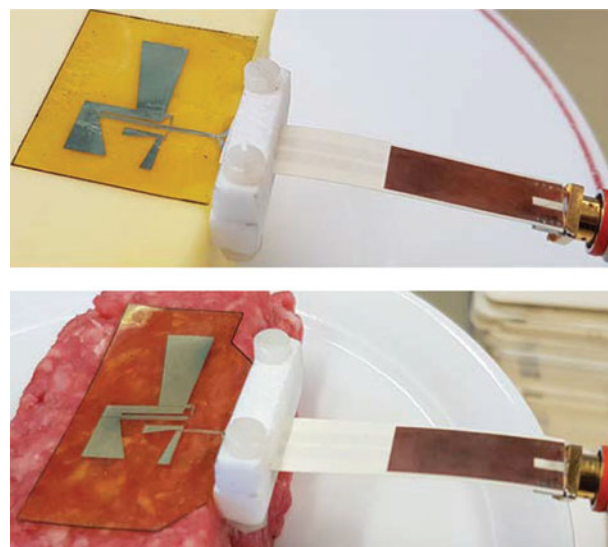| Parameters	Air	Butter	Minced meat
Dielectric constant	1	3.95	42
Loss tangent	0	0.05	0.37

Figure 5. Photos of the two measurement setups with block of butter (upper photo) and block of minced meat (lower photo) attached to the antenna [1].

as extracted material for the backside cover of the model views to investigate the impact of the image eddy current within the conducting backside material in extreme cases.

Chip-film patch process

The newest developed antenna and its RF-chip were produced using the chip-film patch (CFP) process, which is specifically developed by the Institut für Mikroelektronik Stuttgart (IMS-CHIPS) and is particularly suitable for manufacturing Hybrid Systems in Foil with a total thickness between 50 μm and 70 μm [18]. This wafer-level processing realizes combining silicon chips with large area electronics, such as organic thin-film transistors, sensors, and antennas with CMOS-compatible equipment. With this CFP technology, the Benzo cyclobutene (BCB) and Polyimide (PI) is built up like a sandwich layer by layer on the carrier substrate (silicon wafer). BCB is built up due to its good adhesion to metal and silicon chips used here as a functional layer. The whole process flow is shown in Fig. 4.

The process begins with the surface treatment of a 6-inch silicon wafer. Adhesion promoters and upon need alignment marks are applied to the wafer in order to ensure the adhesion of the PI and high accuracy of the litho-processes. After the first spin coating of polymer layer, thin chips are placed in the previously produced cavities using a fine placer. In order to achieve good homogeneity of the polymer layer and good interconnection of the chips, certain requirements regarding cavity depth, process tolerance, and a material filling in cavity trenches under the action of capillary force should and can be approached. In this case, 12 μm cavity depth and 40 μm distance between the cavity side and the chip edge were determined as the optimum [11]. The chips are then embedded by PI and BCB coatings, followed by structuring using a laser
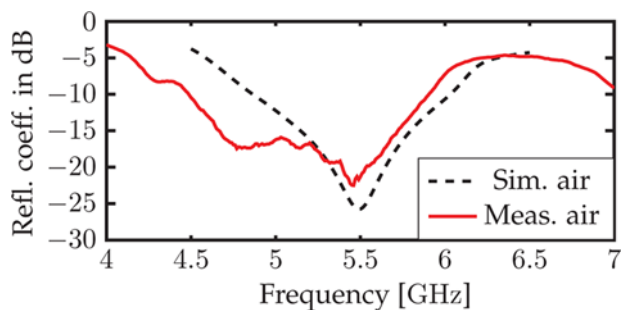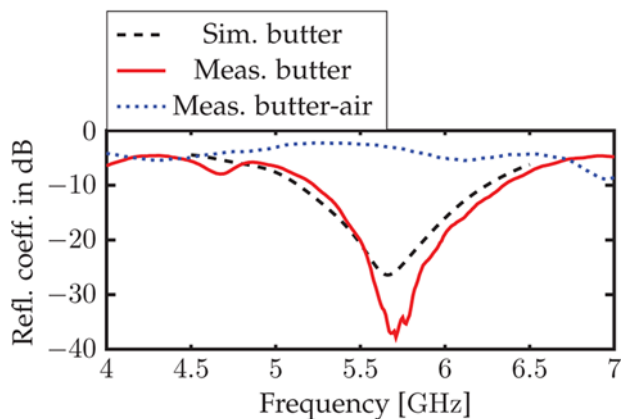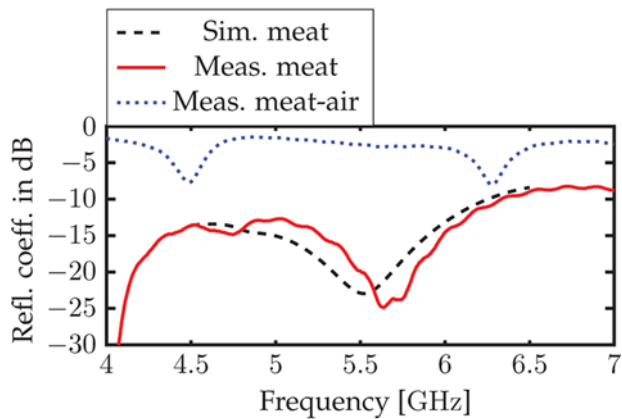
Figure 6. The simulated and measured reflection coefficient over frequency [1]. (a) All in air, (b) on a block of butter ($\epsilon_r = 3.95$), and (c) on a block of minced meat ($\epsilon_r = 42$). For (b) and (c), the blue dotted curve indicates measurement in air, i.e., dielectric block removed.

Figure 7. Die photo of the power amplifier.

Figure 8. Simulated and measured |**S21**| of the PA on rigid Si substrate.
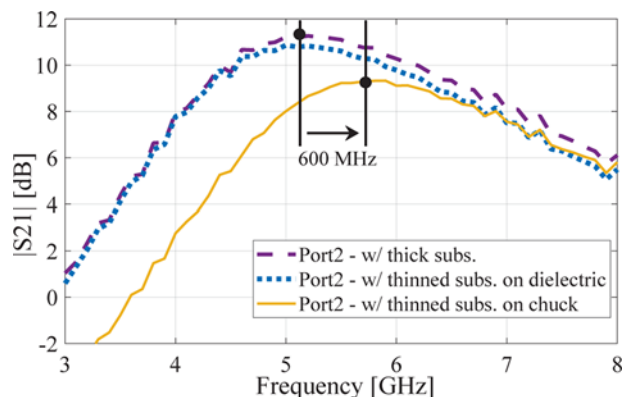
Figure 9. Measured |**S21**| of the PA before and after thinning.

direct writer (VPG400, Heidelberg Instruments) and plasma etching with CF_4 and O_2 (PlasmalabSystem100, Oxford Instruments). Afterwards, AlSiCu is sputtered onto the BCB layer and then lithographically structured in order to connect the chips to antenna and creating outer pads on the foil for later contact.

Stand-alone prototype of the antenna

Before simulating and designing the antenna, the dielectric properties of the chosen materials, butter and minced meat, are
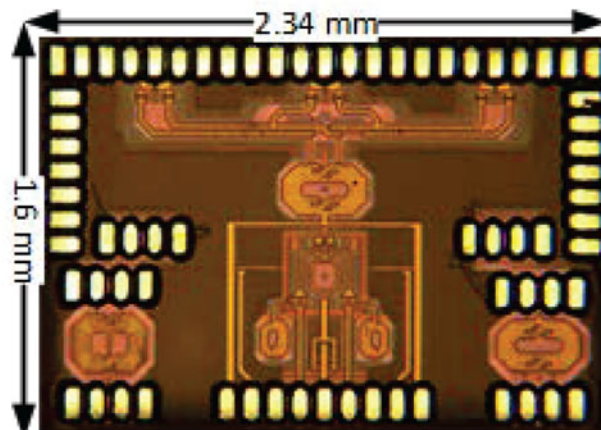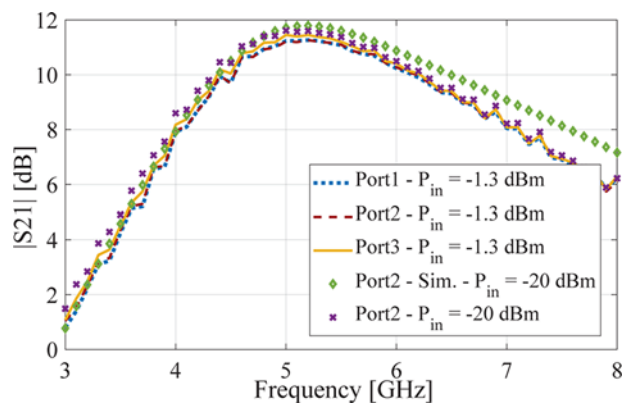
determined. The materials are placed in a section of rectangular waveguide (WR159) and the reflection/transmission parameters are measured. These measurements are then modeled using field simulation software and by fitting the simulation results to the measurements; the dielectric parameters of the materials are determined in the frequency range between 5 and 6 GHz. The extracted material properties are listed in Table 1. These materials are chosen as examples because their properties (loss and dielectric constant) cover a wide range of organic materials related to humans and animals.

Figure 10. The block diagram of the test setup, which is needed for measurements in the anechoic chamber. It comprises an RF unbalance-to-balance (UnBal) transition, a DC-switch board to control the switches of the RF-chip, a DC-bias board for the PA in the chip, and the RF-chip connected to the triple-fed antenna.
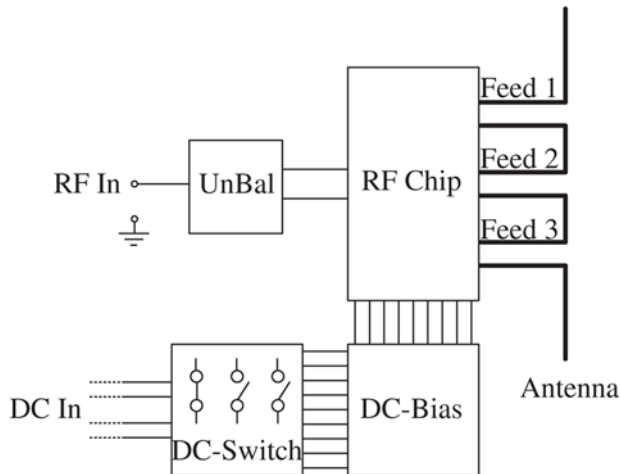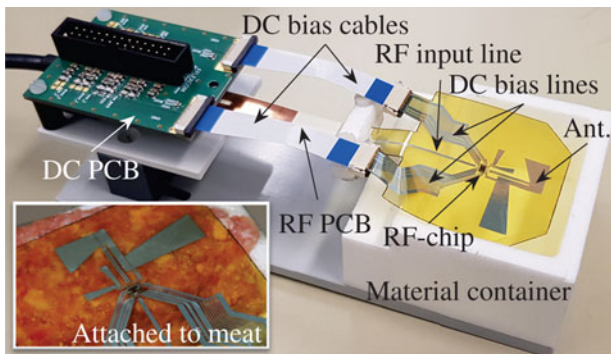

Figure 11. Photograph of the antenna connected to the RF-chip and embedded into polymer foil. The whole system is mounted on a holder for radiation pattern measurement. The inset picture shows the foil system attached to the minced meat–filled material container.

The antenna concept serves as starting point for optimization since the theoretical consideration does not take into account any coupling effects. Also the bandwidth is increased by tapered arms and the overall area (circumferential rectangle) is reduced to $28 \times 15\,\text{mm}^2$ by bent and intertwined features. Figure 1 shows the layout of the proposed antenna. Well-defined balanced feedlines pass from the dipole feed-ports to the chip. The feed-ports are on a straight line, distanced by 0.7 mm.

A prototype of the antenna is manufactured for stand-alone (without RF-chip) measurement. Therefore, three different versions of the antenna board (for different environments: air, butter, and minced meat) are produced. They are identical except for the corresponding $100\,\Omega$ differential feedline. The other feedlines are short-circuited at the locations, where the switches would be in the chip. The feedline of the antenna is extended to the edge of the foil. There, a pressure based foil-to-printed circuit board (PCB) transition connects the foil to a PCB. This PCB contains an unbalanced-to-balanced (UnBal) transition for one-port measurement. Figure 5 depicts two photographs of the one-port reflection coefficient measurement when the antenna is attached to dielectric blocks of butter and meat, respectively.
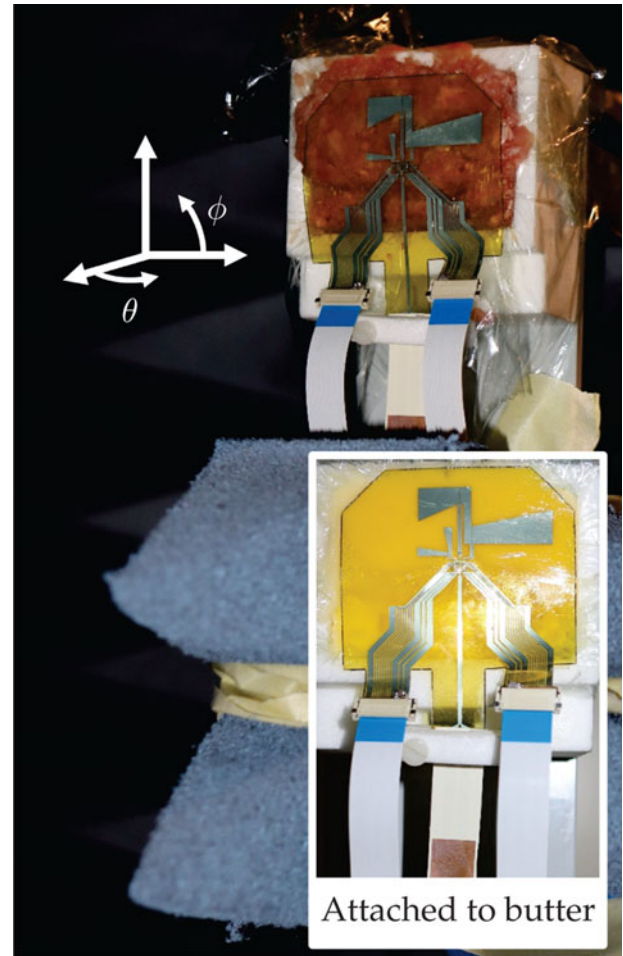

Figure 12. Photo of the system measurement setup and the coordinate system.

The measured reflection coefficient magnitudes are shown in Fig. 6, along with the simulated results. The antenna is well-matched in all three scenarios. The cases with attached dielectric blocks, a separate measurement, shows that the feed match disappears when this particular fed structure is exposed to free-space (when the butter and meat are removed, these are the curves labeled "butter–air" and "meat–air," respectively).

Stand-alone prototype of the RF-chip

The die photo of the chip is shown in Fig. 7, and its dimension is $1.6 \times 2.34\,\text{mm}^2$. The circuit operates with a 1.5 V voltage supply, and the power consumption is around 75 mW. Stand-alone PA measurement is realized using GSGSG RF wafer probes. Moreover, an external balun is used for the ports because of a single-ended two-port VNA. Figure 8 shows that all three output ports of PA individually provide approximately the same gain, and post-layout simulation results are verified with the experimental results. The measured minimum gain of the PA on the metal chuck is about 10 dB in the required frequency band before thinning. In addition, the simulated output power at the 1 dB compression point is 11.6 dBm with a power-added efficiency (PAE) of 17.5% at 5.5 GHz. The input power of the PA is set to −1.3 dBm after the losses due to the external balun and wafer probe because of the maximum VNA output power of 0 dBm. Hence, PA saturation
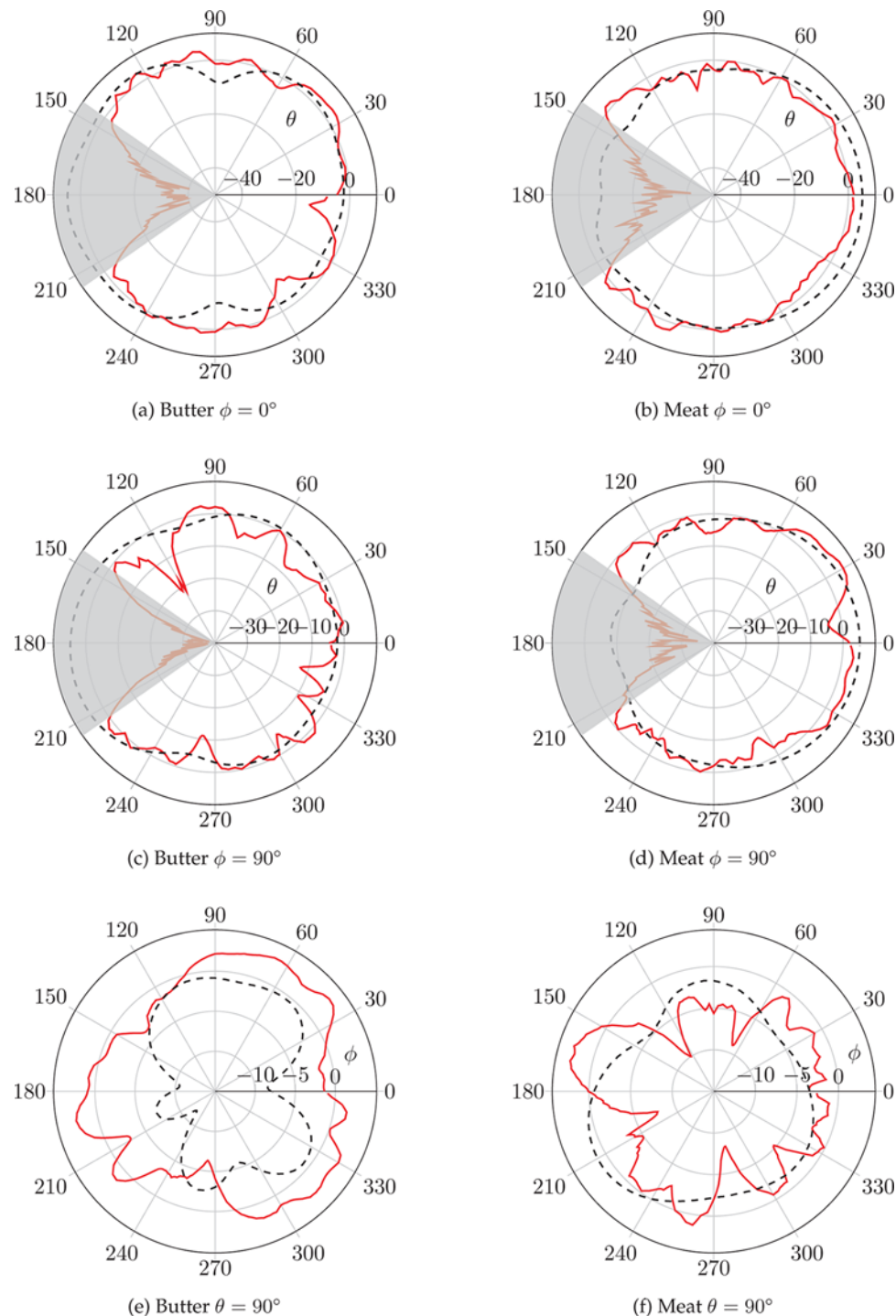
Figure 13. Polar plots of the specific cut planes (see captions of the sub figures) of the measured (red line) and simulated (gray dashed line) radiation pattern. The light gray areas in subfigures (a)–(d) indicate the angle range, where all the radiated power is dissipated in the absorbers of the rotating arm of the anechoic chamber.

is prevented. As illustrated in Fig. 9, the measured peak gain frequency of the thinned PA on the conductor material (metal Thermo-Chuck) shifts about 600 MHz toward higher frequencies compared to the thin silicon chip on dielectric material and the thick silicon chip. The significant frequency difference is due to the image mirror current within the conducting material [19]. Despite the thin substrate of the chip, no significant S-parameter

degradation was observed in the measurements realized on the dielectric material (FR4).

Previous studies also evaluated the RF performance of the PA chip embedded in the polyimide foil [13]. The recent implementation of thinned Si PA on a 1 µm-thick AlSiCu heat spreader in foil substrate shows that the patterned heat spreader instead of the solid one can be used to prevent the image mirror currents

induced in the heat spreader due to the magnetic field of the passives [19].

Prototype of the system

A prototype of the 3-port antenna connected to an RF-chip embedded in polymer foil, as described in the section "Chip-film patch process," is manufactured. Since the respective output port (that is active) and the input port of the antenna are designed to have 100 Ω differential impedance, power matching between the antenna and the RF-chip is obtained.

A DC-bias and DC-switch PCB is developed to conveniently bias and control the switches of the RF-chip in the foil. To connect the DC PCB with the foil, flat flexible cables (FFC) with clamp connectors are used. The RF input line on the foil of the chip is separated and connected to a RF-PCB, which includes a foil-to-PCB transition and a UnBal. This is the same as described in the subsection "Stand-alone prototype of the antenna." A block diagram of the test setup is depicted in Fig. 10. All of these components are then mounted to a holder for radiation pattern measurement. To test the antenna on different materials, a material container out of EM transparent foam (ROHACELL) is used. A photograph is depicted in Fig. 11. The inset picture shows the setup when the material container is filled with minced meat and the antenna is attached to it.

The whole system is placed in an anechoic chamber to measure the radiation pattern for the cases of butter and minced meat. The three-dimensional radiation pattern is measured in the far field using a spherical scanner, and the directivity is determined by referencing each measured point to the total radiated power (obtained by integrating the entire pattern) divided by the spherical surface area (4π). On the DC-switch board, manual switches are implemented for the adjustment of the right output port of the RF-chip, which is the input port of the antenna. The DC voltage sources are placed beneath absorbers on the rotating stand of the anechoic chamber so that they can rotate during the measurement. In the photograph of Fig. 12, the foil system attached to the two different materials and the coordinate system to which all the measurement results refer are shown. It should be noted that this radiation pattern measurement serves as a verification of the system communication functionality only. Since the main focus in this antenna design is to reduce the reflection coefficient at different ports for either scenario, it is not of interest how the radiation occurs. Beside this, the DC lines and cables as well as the DC PCB will alter the pattern. In Fig. 13, some cut planes of the measured (red curve) and simulated (dashed gray curve) radiation pattern are shown. Note, the simulation results shown here are without any surrounding lines or cables or PCB. The light gray areas in subfigures (a)–(d) indicate the angle range, where all the radiated power is dissipated in the absorbers of the rotating arm of the antenna positioning system. Obviously, the measurement results show a similar course when compared with simulations, but ripples are clearly visible in the measurements. This stems from the conductive interference elements (e.g. DC lines and cables) in the vicinity of the antenna.

Conclusion

A design approach for a triple-fed antenna connected to an RF-chip was presented. Furthermore, a prototype was made, which in turn shows that the approach leads to the desired goal, which is adaptivity to different scenarios. The antenna shows well-matched feed impedance for three different environmental scenarios, that is, when placed in free-space, when attached to a block of permittivity of about 4, and when attached to a block of permittivity of about 42. In all three scenarios, the measured feed match is better than −20 dB at 5.5 GHz. It was also shown that the antenna is functional with a specially made RF-chip incorporated in a thin polymer foil. Thereby, the RF-chip provides the switching capability. Thus, this lays the foundation for a highly flexible wireless transmission system.

The proposed concept can be adapted to other sets of EM environments. However, more than three scenarios, meaning more than three feeds, seems too involved, and its feasibility is questionable with the given approach.

Competing Interests. The authors report no conflict of interest.

References

1. **Fischer SB, Wang S, Hesselbarth J and Burghartz JN** (2022) Flexible and adaptive dipole-based triple-fed antenna for single-chip transceiver. *2022 16th European Conference on Antennas and Propagation (EuCAP)*. Madrid, Spain, 1–5. doi: 10.23919/EuCAP53622.2022.9769337.

2. **Ferreira D, Pires P, Rodrigues R and Caldeirinha RFS** (2017) Wearable textile antennas: Examining the effect of bending on their performance. *The IEEE Antennas and Propagation Magazine* **59**(3), 54–59.

3. **Haj-Omar A, Thompson WL, Kim Y, Glick P, Tolley M and Coleman TP** (2016) Stretchable and flexible adhesive-integrated antenna for biomedical applications. *IEEE International Symposium on Antennas and Propagation (APSURSI)* IEEE, 459–460.

4. **Soares A, Fonseca S and Giarola A** (1984) The effect of a dielectric cover on the current distribution and input impedance of printed dipoles. *IEEE Transactions on Antennas and Propagation* **32**(11), 1149–1153.

5. **Dissanayake T, Esselle KP and Yuce MR** (2009) Dielectric loaded impedance matching for wideband implanted antennas. *The IEEE Transactions on Microwave Theory and Techniques (T-MTT)* **57**(10), 2480–2487.

6. **Nikolayev D, Zhadobov M, Karban P and Sauleau R** (2016) Increasing the radiation efficiency and matching stability of in-body capsule antennas, *10th European Conference on Antennas and Propagation (EuCAP)* IEEE.

7. **Gu Q and Morris AS** (2013) A new method for matching network adaptive control. *The IEEE Transactions on Microwave Theory and Techniques (T-MTT)* **61**(1), 587–595.

8. **Rasteh M and Hesselbarth J** (2018) Dipole antenna with multiple feeds adapting to the environment. *IEEE Asia-Pacific Conference on Antennas and Propagation (APCAP)* IEEE, 38–41.

9. **Fischer SB and Hesselbarth J** (2020) A single-layer planar antenna unaffected by a possibly close-by metal surface. *14th European Conference on Antennas and Propagation (EuCAP)* IEEE, 1–5.

10. **Zhang T, Hou Z, Johnson RW, Del Castillo L, Moussessian A, Greenwell R and Blalock BJ** (2009) Flexible electronics: Thin silicon die on flexible substrates. *IEEE Transactions on Electronics Packaging Manufacturing* **32**(4), 291–300.

11. **Wang S, Albrecht B, Harendt C, Schulze Spüntrup JD and Burghartz JN** (2021) Ultra-thin image sensor chip embeded foil. *IEEE International Conference on Flexible and Printable Sensors and Systems (FLEPS)* IEEE, 1–4.

12. **Özbek S, Grözing M, Alavi G, Burghartz JN and Berroth M** (2018) Three-path SiGe BiCMOS LNA on thinned silicon substrate for IoT applications. *13th European Microwave Integrated Circuits Conference (EuMIC)* IEEE, 273–276.

13. **Alavi G, Özbek S, Rasteh M, Grözing M, Berroth M, Hesselbarth J and Burghartz JN** (2019) Toward a flexible and adaptive wireless hub by embedding power amplifier thinned silicon chip and antenna in a polymer foil. *International Journal of Microwave and Wireless Technologies* **11**(9), 864–871.

14. **Saoudy S and Hamid M** (1987) Optimal design of multiply fed dipole antennas. *IEEE Transactions on Antennas and Propagation* **35**(9), 1001–1009.

15. **King R** (1950) Asymmetrically driven antennas and the sleeve dipole. *Proceedings of the IRE* **38**(10), 1154–1164.

16. **Fischer SB and Hesselbarth J** (2021) Off-centre fed dipole suppressing the radiation of the feedline by a load impedance at an arbitrary point. *15th European Conference on Antennas and Propagation (EuCAP)* IEEE, 1–5.

17. **Özbek S, Alavi G, Digel J, Grözing M, Burghartz J and Berroth M** (2018) 3-Path SiGe BiCMOS power amplifier on thinned substrate for IoT applications. *Integration* **63**, 291–298.

18. **Albrecht B, Alavi G, Elsobky M, Ferwana S, Passlack U, Harendt C and Burghartz JN** (2018) Multi-chip patch in low stress polymer foils based on an adaptive layout for flexible sensor systems. *7th Electronic System-Integration Technology Conference (ESTC)* Dresden, Germany: IEEE.

19. **Özbek S, Wang S, Fischer SB, Grözing M, Burghartz JN and Hesselb J** (2022). Integrating ultra-thin SiGe BiCMOS power amplifier chip in combination with flexible antenna in the polymer foil. *2022 IEEE International Symposium on Circuits and Systems (ISCAS)* IEEE.

Serafin B. Fischer-Kennedy was born in Buchholz in der Nordheide, Germany, in 1991. He received the B.Sc. and M.Sc. degree in electrical engineering from University of Stuttgart, Germany, in 2016 and 2018, respectively. He is currently pursuing the Ph.D. degree at the University of Stuttgart, Stuttgart, Germany. His current research interests include matching networks, adaptive antennas, and antenna-arrays.

Sefa Özbek received the B.Sc. degree in electrical engineering from the Fatih University, Istanbul, Turkey, in 2007 and the M.Sc. degree with a focus on electronics engineering from University of Stuttgart, Stuttgart, Germany, in 2012. Since 2015, he has been pursuing the Ph.D. degree at the Institute of Electrical and Optical Communication Engineering, University of Stuttgart. His research interests include the design of front-end transceiver components in SiGe BiCMOS for IoT applications. Sefa Özbek worked as an IC design engineer with DMCE, Linz, Austria, from 2012 to 2015.

Shuo Wang was born in Qingdao, China, in 1987. He received M.Sc. degrees in electrical engineering from TU Dresden, Germany, in 2014. From 2015 to 2017, he was a Processing Engineer with EV Group E. Thallner GmbH, St. Florian am Inn, Austria. Since 2018, he worked as a Ph.D. student at IMS CHIPS Stuttgart and is currently pursuing the Ph.D. degree at the University of Stuttgart, Stuttgart, Germany. His current research interests include Hybrid System-in-Foil, Semiconductor Process Technology.

Markus Grözing received the Dipl.-Ing. and the Dr.-Ing. degrees from the University of Stuttgart in 2000 and 2007, respectively. During his doctoral study, his research was focused on phase noise and jitter in ring oscillators and on mixed-signal CMOS ciruit design. Since 2007, he leads the integrated circuit design group at the Institute of Electrical and Optical Communications Engineering at the University of Stuttgart. His current research topics are high-speed transmitters and receivers for serial links as well as gigasample-range analog-to-digital and digital-to-analog converters in CMOS and BiCMOS technologies. He has authored or co-authored more than 70 scientific papers and he has served as a reviewer for IEEE TMTT, JSSC, TCAS-II, JLT, and TVLSI.

Jan Hesselbarth was born in Dresden, Germany, in 1970. He received the Ph.D. degree from the Swiss Federal Institute of Technology (ETH), Zurich, Switzerland, in 2002. From 2001 to 2005, he was a Design Engineer with Huber+Suhner, Pfaffikon, Switzerland. From 2005 to 2008, he was a Technical Staff Member with Bell Laboratories, Dublin, Ireland. He was a Senior Researcher and Lecturer with ETH Zurich. Since 2011, he has been a Professor with the Institute of Radio Frequency Technology, University of Stuttgart, Stuttgart, Germany. His current research interests include antennas and millimeter-wave circuits and packaging.

Manfred Berroth was born in Obersontheim, Germany, in 1956. He received the Dipl.-Ing. degree from the University of the Federal Armed Forces, Munich, Germany, in 1979 and the Ph.D. (Dr.-Ing.) degree from Ruhr-Universität Bochum, Bochum, Germany, in 1991. In 1987, he joined the Institute for Applied Solid State Physics, Freiburg, Germany, where he was engaged in the development of circuit simulation models for GaAs field-effect transistors, as well as integrated circuit design. In 1995, he became the Deputy Director of the Institute for Applied Solid State Physics, Freiburg, Germany. Since 1996, he is a Full Professor and the Head of the Institute of Electrical and Optical Communication Engineering, University of Stuttgart, Stuttgart, Germany. His research interests are modeling and characterization of electronic and opto-electronic devices and integrated circuits.

Joachim N. Burghartz was born in Aachen, Germany, in 1956. He studied electrical engineering at RWTH Aachen and graduated (Dipl.-Ing.) in 1982. In 1987, he received his Ph.D. (Dr.-Ing.) from Universität Stuttgart. From 1987 until 1998, he worked at the IBM Thomas J. Watson lab in Yorktown Heights, NY, USA. From 1998 until 2005, he was Full Professor at TU Delft and headed the High-Frequency Technology and Components (HiTeC) research team. Since October 2005, Prof. Dr. Burghartz has been Director and Chairman of the Board at Instituts für Mikroelektronik Stuttgart (IMS CHIPS) as well as being Full Professor at Universität Stuttgart. He has also been heading the Institute for Nano and Microelectronic Systems (INES) at Universität Stuttgart since March 1, 2006. August 18, 2013, marked his launch as Manager of the IMS Mikro-Nano Produkte GmbH.